Liu et al. *Zool. Res.* 2025, 46(5): 1175–1186
https://doi.org/10.24272/j.issn.2095-8137.2025.018
https://cstr.cn/32248.14.zr.2025.018

ZR | Zoological Research

Article Open Access

Coordinated inhibition of M1 macrophage polarization by FIT2-mediated lipid droplet biosynthesis and FABP5

Yi-Han Liu[1], Bei Li[1], Yuan-Xing Zhang[3,4], Sang Ho Choi[2], Shuai Shao[1,3,4,*], Qi-Yao Wang[1,3,4,*]

[1] *State Key Laboratory of Bioreactor Engineering*, *East China University of Science and Technology*, *Shanghai* 200237, *China*

[2] *National Research Laboratory of Molecular Microbiology and Toxicology*, *Department of Agricultural Biotechnology*, *Seoul National University*, *Seoul* 151-742, *Republic of Korea*

[3] *Laboratory of Aquatic Animal Diseases of MARA*, *Shanghai* 200237, *China*

[4] *Shanghai Engineering Research Center of Maricultured Animal Vaccines*, *Shanghai* 200237, *China*

ABSTRACT

Lipid droplets (LDs) serve as dynamic organelles central to host immune response and bacterial infection resistance by recruiting multiple proteins and peptides with established antiviral and antibacterial properties. Although macrophage polarization is integral to both innate immunity and lipid homeostasis, the regulatory influence of LDs on this process remains unclear. In this study, augmentation of LDs via oleic acid (OA) treatment attenuated M1 polarization in RAW264.7 macrophages. Given that LD budding is mediated by fat storage-inducing transmembrane protein 2 (FIT2) encoded by *FITM2*, transcriptomic analysis following *FITM2* knockdown revealed suppressed expression of fatty acid-binding protein 5 (FABP5), a lipid-binding protein that further modulated LD abundance. Both FIT2 and FABP5 were found to regulate LD content and collectively contributed to inhibition of M1 macrophage polarization. This shift impaired macrophage capacity to mount effective antibacterial responses. These findings identify a coordinated role for LDs and FABP5 in modulating M1 macrophage polarization, establishing a mechanistic link between lipid metabolism and innate host defense against bacterial infection.

Keywords: Macrophage polarization; Lipid droplet; FABP5; FIT2

INTRODUCTION

Lipid droplets (LDs) are dynamic globular organelles that bud from the endoplasmic reticulum and undergo growth and maturation (Walther et al., 2017; Zechner et al., 2012). Beyond their classical roles in lipid storage, metabolic regulation, and intracellular trafficking, LDs contribute to signal transduction processes and immune modulation (Olzmann & Carvalho, 2019; Zhang et al., 2017). LDs function as metabolic reservoirs exploited by intracellular pathogens but also act as immunological platforms that orchestrate host antibacterial responses (Bosch et al., 2020; Hüsler et al., 2023; Walther et al., 2017). Given these opposing roles, elucidating the regulatory function of LDs within pathogen-host interactions remains a critical area of investigation.

Macrophage function is highly dependent on intrinsic cellular metabolism (Yan & Horng, 2020). In response to environmental cues, macrophages adopt polarized phenotypes along a continuum, including classically activated M1 and alternatively activated M2 states (Chen et al., 2020). Co-stimulation with lipopolysaccharide (LPS) and interferon-γ (IFN-γ) drives M1 polarization, characterized by heightened proinflammatory activity (Ivashkiv, 2013; Sica & Mantovani, 2012). Upon LPS stimulation, fatty acid synthesis in macrophages is enhanced through the induction of Toll-like receptor 4 (TLR4) and reduction of NADPH biosynthesis, thereby promoting inflammatory responses (Yan & Horng, 2020). Furthermore, disruption of lipolytic pathways, such as loss of adipose triglyceride lipase or its co-activator comparative gene identification-58, attenuates the phagocytic capacity of macrophages (Goeritzer et al., 2014). In contrast, persistent M2 polarization contributes to chronic infection and promotes cancer-associated immunosuppression (Noy & Pollard, 2014; Russell et al., 2019). These context-dependent effects underscore the therapeutic relevance of selectively modulating macrophage polarization while minimizing detrimental outcomes (Boutilier & Elsawa, 2021). For instance, loss of aconitate decarboxylase 1, a key enzyme in itaconate synthesis, exacerbates M1 polarization and atherosclerosis in myeloid cells, while treatment with 4-octyl itaconate suppresses M1 polarization and alleviates disease progression via nuclear

Received: 24 March 2025; Accepted: 24 April 2025; Online: 25 April 2025

Foundation items: This work was supported by the National Key Research and Development Program (2022YFE0101200), National Natural Science Foundation of China (32130108), and China Agriculture Research System of MOF and MARA (CARS-47)

*Corresponding authors, E-mail: shaoscott@ecust.edu.cn; oaiwqiyao@ecust.edu.cn

factor erythroid 2-related factor 2 (Nrf2) activation (Song et al., 2023).

Fatty acid-binding protein 5 (FABP5) is a cytosolic lipid chaperone closely linked to LD formation and maintenance (Karanth et al., 2008). FABP5 binds to and transports free fatty acids to intracellular regions for energy production and biosynthetic metabolism (Furuhashi & Hotamisligil, 2008; Lee et al., 2018a; O'Sullivan & Kaczocha, 2020). In acute myeloid leukemia (AML) cells, FABP5 sustains LD abundance, thereby supporting cell viability and protecting against apoptosis (Liang et al., 2023). In LPS-stimulated bone marrow-derived macrophages, FABP5 deficiency results in intracellular accumulation of unsaturated fatty acids, activation of AMP-activated protein kinase, and suppression of the NF-κB signaling pathway, ultimately enhancing inflammatory responses (Hou et al., 2022a). These findings indicate that FABP5 influences immune regulation beyond its established role in lipid transport and signaling.

M1 polarization of macrophages is essential for maintaining cellular homeostasis in response to bacterial infection (Lumeng et al., 2007). Although LDs are known to supply lipid precursors required for the synthesis of inflammatory mediators, such as phospholipids, eicosanoid-derived leukotrienes, and prostaglandins (Yan & Horng, 2020), their regulatory effect on macrophage polarization remains poorly defined. OA-driven LDs are enriched in triacylglycerols and monounsaturated fatty acids and are associated with the generation of anti-inflammatory lipids that activate peroxisome proliferator-activated receptor γ (PPARγ) and suppress NF-κB signaling, promoting M2 polarization (Yan & Horng, 2020). In the context of metabolically associated steatohepatitis (MASH), LDs released from damaged hepatocytes initially serve as inflammatory danger signals. However, prolonged exposure to these LDs robustly attenuates proinflammatory signaling, diminishing the stimulatory effects of LPS and IFN-γ on cytokine expression and NLRP3 inflammasome activation (Zhou et al., 2025). Therefore, the intrinsic mechanisms by which LDs influence macrophage polarization must be interpreted within clearly defined environmental frameworks and contexts.

Fat storage-inducing transmembrane protein 2 (FIT2), encoded by *FITM2*, promotes LD biogenesis through interaction with the cytoskeletal protein Septin 7, facilitating the formation of cytoplasmic ring-like structures on endoplasmic reticulum tubules that enable LD budding (Chen et al., 2021; Kadereit et al., 2008). To evaluate the role of LDs in macrophage polarization, *FITM2* knockdown was used to reduce LD abundance and evaluate its impact on M1 activation. Transcriptomic profiling revealed that LD depletion down-regulated *FABP5* expression, which, in turn, inhibited M1 polarization. Altered M1 polarization modulated the capacity of macrophages to respond to pathogen infection. These findings establish a regulatory axis involving FIT2-FABP5-LD that influences macrophage inflammatory status and offer a potential strategy for controlling pathogen susceptibility through targeted modulation of lipid metabolism.

MATERIALS AND METHODS

Culture of bacterial strains and macrophage cells

All bacterial strains and plasmids used in this study are presented in Supplementary Table S1, and the primers are listed in Supplementary Table S2. *Edwardsiella piscicida* EIB202, *Escherichia coli* DH5α, and *Salmonella enterica* subsp. *enterica* serovar Typhimurium SL1344 were cultured in Luria Bertani (LB) medium at 30°C or 37°C. RAW264.7 macrophage cells were cultured in Dulbecco's Modified Eagle Medium (DMEM) supplemented with 10% fetal bovine serum (FBS) at 37°C in a humidified incubator containing 5% CO_2.

For M1 polarization, RAW264.7 cells were treated with 100 ng/mL LPS (Beyotime, ST1470, China) and 20 ng/mL IFN-γ (Beyotime, P5664, China) for 12 h. To assess the influence of lipid accumulation, cells were exposed to 10 μmol/L OA (MCE, HY-N1446, China) during polarization.

RNA interference (siRNA) assay

RNA interference was performed using RNATransMate transfection reagent (Sangon, E607402, China). Briefly, 10 μL of RNATransMate was added to 190 μL of Opti-MEM medium (Thermo Fisher, 31985070, USA). Separately, 2 μL (40 pmol) of gene-specific siRNA (Sangon, China) (Supplementary Table S2) was diluted in 200 μL of Opti-MEM and incubated for 10 min. The combined mixture was added to each well containing 400 000 RAW264.7 cells.

RNA extraction and RT-qPCR analysis

To determine the mRNA level of corresponding macrophage markers, total RNA was extracted from RAW264.7 cells using an RNA isolation kit (BioFlux, BSC52M1, China) according to the manufacturer's protocols. Reverse transcription was conducted immediately using a FastKing RT kit (TRANSGEN BIOTECH, S61204-V3, China) to synthesize cDNA. Three independent RT-qPCR experiments were performed using the Applied Biosystems 7500 Real-Time System (USA). Relative transcript levels were determined using the comparative CT method and normalized to β-actin as the internal reference gene. All primers used for RT-qPCR are listed in Supplementary Table S2.

RNA sequencing (RNA-seq) and transcriptome analysis

To evaluate transcriptomic changes, *FITM2* expression was silenced in RAW264.7 cells, followed by co-stimulation with LPS and IFN-γ for 12 h in both si-*FITM2* and scrambled siRNA control groups. Total RNA was extracted from ten million cells and subjected to RNA-seq (Personalbio, China). High-quality reads were aligned to the reference genome of the species, and gene expression levels were quantified. Transcripts with fragments per kilobase of transcript per million mapped reads (FPKM) greater than 1 were retained for downstream analysis. Fold changes were calculated by comparing FPKM values across groups. Differential expression and enrichment analyses were subsequently carried out based on these results.

Western blot (WB) analysis

To evaluate the expression of corresponding macrophage markers, cell pellets were collected by centrifugation at 1 000 r/min for 5 min. Lysis buffer (YEASEN, 20315S05, China) and double-distilled water were added to the pellets at a ratio of 1 mL lysis buffer per 1×10^7 cells. Lysates were boiled at 95°C for 10 min, separated using 4%–20% polyacrylamide gradient gels (Smart-Lifesciences, SLE019, China), and transferred to polyvinylidene fluoride (PVDF) membranes (Millipore, BM4AB8360A, USA). The membranes were then incubated in 10% skim milk prepared in phosphate-buffered saline (PBS) containing 0.05% Tween-20 (PBST) for 2 h, followed by incubation with primary antibodies in PBST for 2 h and

secondary antibodies in PBST for 1.5 h. Antibodies against TNF-α, Arg-1, and iNOS were used. β-actin served as the internal control.

Enzyme-linked immunosorbent assay (ELISA)

Secretion levels of macrophage markers were assessed by quantifying TNF-α and IL-6 in cell culture supernatants using QuantiCyto® Mouse TNF-α (NeoBioscience, EMC102a.96, China) and IL-6 ELISA kits (NeoBioscience, EMKC006.96, China). Briefly, cell culture supernatants were collected and centrifuged at 1 000 r/min for 5 min. Samples were diluted 10-fold and added to blank wells (100 μL/well), then incubated at 37°C in a constant temperature incubator for 90 min. After that, 100 μL of biotinylated antibody working solution, enzyme conjugate working solution, substrate solution (TMB), and stop solution were sequentially added. Optical density at 540 nm (OD_{540}) was subsequently measured.

Neutral red staining and reactive oxygen species (ROS) measurement

Lysosomal activity of the cells was assessed using a Neutral Red Staining kit (Beyotime, C0037, China). Cells were cultured in 96-well plates (200 μL/well), and 20 μL/well of neutral red staining solution was added and incubated for 2 h. The cells were washed twice with PBS, followed by the addition of 200 μL/well of neutral red detection lysate. Absorbance was measured at 540 nm.

Intracellular ROS levels were measured using a ROS detection kit (Beyotime, S0033S, China). 2',7'-Dichlorodihydrofluorescein diacetate (DCFH-DA) was first diluted 1:1 000 in serum-free medium to a final concentration of 10 μmol/L and added to the cells. After 20 min of incubation at 37°C, cells were washed three times with PBS. Fluorescence intensity was quantified via flow cytometry using FITC-A absorbance.

Fluorescence microscopy

To assess LD abundance, RAW264.7 cells were cultivated in 24-well plates at a density of 1.0×10^5 cells/well. BODIPY™ FL C16 (Thermo Fisher, D3821, USA) was added at a 1:1 000 dilution and incubated for 30 min. After two PBS washes, cells were fixed in 4% paraformaldehyde for 15 min and stained with 4',6-diamidino-2-phenylindole (DAPI, Beyotime, C1005, China) for 5 min. Images were taken using confocal microscopy (A1R, Nikon, USA) and fluorescence intensity was determined using ImageJ.

Bacterial infection assay

RAW264.7 cells were cultivated in 6-well plates at a density of 1×10^6 cells/well and allowed to adhere overnight. Overnight bacterial cultures were washed three times with PBS and used to infect cells at a multiplicity of infection (MOI) of 10. After 2 h of incubation, the cells were washed twice with PBS and then exposed to a medium containing 1 000 μg/mL of gentamicin for 15 min at 35°C to eliminate extracellular bacteria.

To quantify intracellular bacteria, the medium was aspirated, and cells were washed twice with sterile PBS, then lysed in 0.5% Triton X-100 for 25 min at 35°C. Lysates were collected, serially diluted in sterile PBS, and plated on agar plates for colony counting. Colony-forming units were normalized to cell numbers to evaluate intracellular bacterial proliferation.

Statistical analysis

Statistical analyses were performed using one-way or two-way analysis of variance (ANOVA) in GraphPad Prism (v.9.5). Differences were considered significant at $^{*}P<0.05$, $^{**}P<0.01$, $^{***}P<0.001$, and $^{****}P<0.001$.

RESULTS

OA inhibits M0 to M1 macrophage polarization

Given the established role of lipid metabolism in shaping macrophage polarization and the capacity of OA to enhance M2 macrophage polarization (Yan & Horng, 2020), the effect of OA on M1 polarization was evaluated in RAW264.7 cells. Cells were treated with 10 μmol/L OA in combination with 100 ng/mL LPS and 20 ng/mL IFN-γ for 12 h (Sica & Mantovani, 2012) to assess potential modulation of M1 activation. Morphological analysis revealed that LPS and IFN-γ co-stimulation induced pronounced M1-like features, whereas simultaneous OA treatment visibly reduced the abundance of M1-polarized cells (Figure 1A). RT-qPCR analysis showed marked up-regulation, ranging from 4- to 20-fold, in transcripts encoding M1 markers (IL-6, iNOS, and TNF-α) following LPS and IFN-γ stimulation, accompanied by a suppression of the transcripts encoding M2 markers (CD206 and Arg-1) (Figure 1B). Co-treatment with OA significantly attenuated the expression of M1 markers, while partially restoring transcription of M2 markers (Figure 1B). Consistent with transcriptomic changes, WB and ELISA confirmed approximately 1.5-fold reductions in TNF-α and iNOS protein expression and diminished secretion of TNF-α and IL-6 in cells treated with OA, LPS, and IFN-γ compared to cells exposed to LPS and IFN-γ alone. In contrast, Arg-1 protein levels were partially restored (Figure 1C–E).

ROS, comprising oxygen-derived free radicals and peroxides, play critical roles in macrophage polarization (Manoharan et al., 2024). Flow cytometric analysis demonstrated elevated ROS production in M1-polarized cells induced by LPS and IFN-γ, which was markedly suppressed by OA co-treatment (Figure 1F). Similarly, intracellular lysosomal activity, a reflection of macrophage polarization (Sergin et al., 2015), was evaluated using neutral red staining. Results indicated that OA treatment led to a notable reduction in lysosomal activity compared to M1-polarized cells (Figure 1G). Together, these results suggest that OA significantly impairs M1 polarization in RAW264.7 macrophages at both transcriptional and functional levels.

Impaired LD formation promotes M1 macrophage polarization

OA is a well-established inducer of LD accumulation, while FIT2, an integral endoplasmic reticulum membrane protein, governs LD budding and maturation (Chen et al., 2021). To investigate the mechanistic link between LD biogenesis and macrophage polarization, *FITM2*, encoding FIT2, was knocked down in RAW264.7 cells using siRNA. RT-qPCR confirmed a robust reduction in *FITM2* transcript levels in the presence of si-*FITM2* (Figure 2A). Likewise, WB analysis of PLIN2, a canonical marker of LD abundance (Griseti et al., 2024), demonstrated markedly diminished PLIN2 expression, indicating effective depletion of LDs in *FITM2* knockdown cells (Figure 2B). Confocal microscopy further corroborated the loss of LD formation in *FITM2* knockdown cells compared to those transfected with scrambled siRNA (Figure 2C, D).

To assess the consequences of impaired LD formation on macrophage polarization, transcript and protein levels of M1

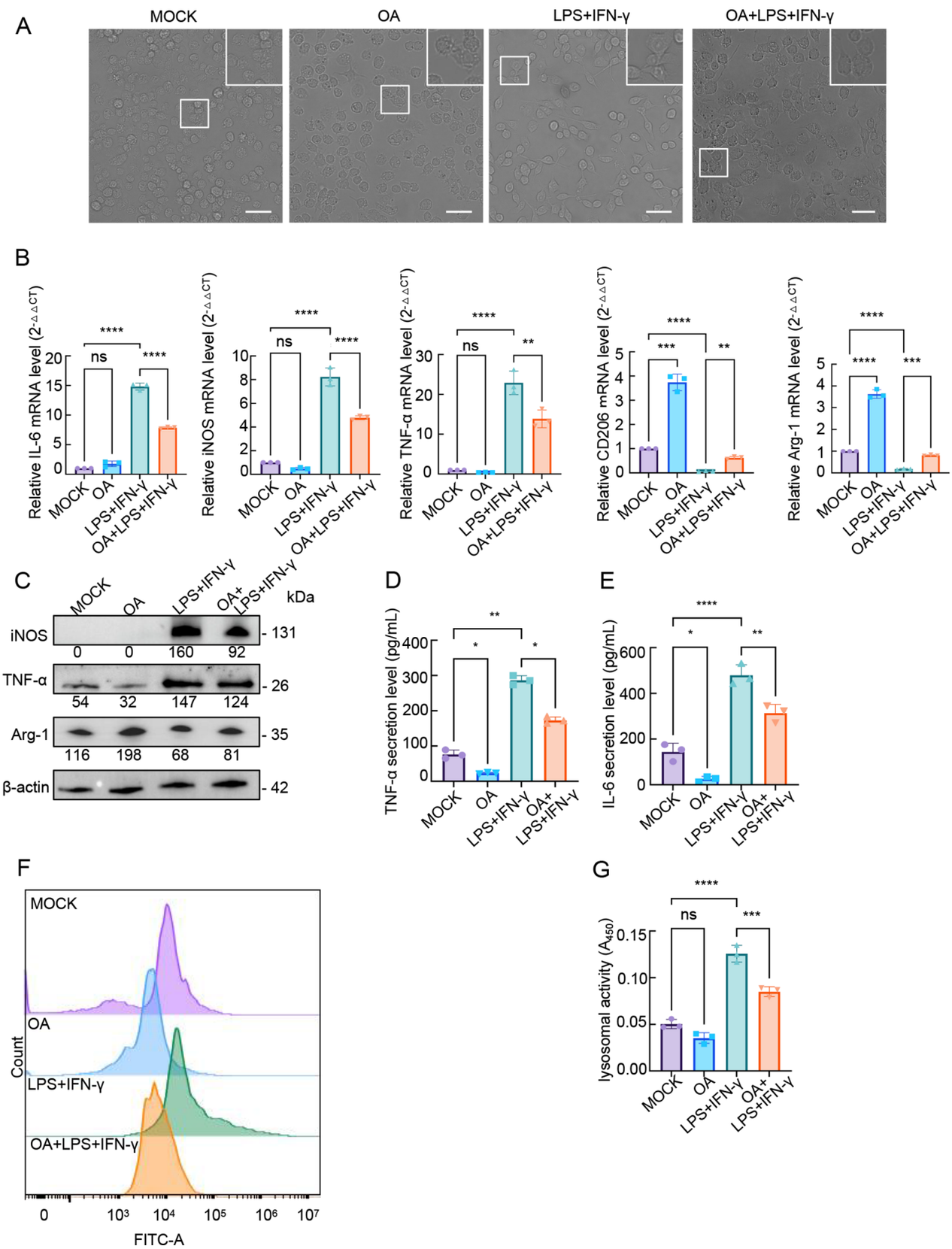

Figure 1 OA inhibits M1 macrophage polarization.

A: Representative morphology of RAW264.7 cells treated with LPS, IFN-γ, and OA for 12 h. Spindle-shaped cells indicate M1 macrophages. All images shown are representative of at least five independent experiments. B: mRNA expression of macrophage polarization markers influenced by OA measured by RT-qPCR. β-actin was used as the internal control. C: Protein expression profiles of macrophage polarization markers measured by western blot. D, E: Cytokine secretion levels of TNF-α and IL-6 measured by ELISA. F: Intracellular ROS levels determined by flow cytometry. G: Lysosomal activity determined by neutral red dye staining. Data are presented as mean±SD. (n=3). *: P<0.1; **: P<0.01; ***: P<0.001; ****: P<0.0001; ns: Not significant, one-way ANOVA.

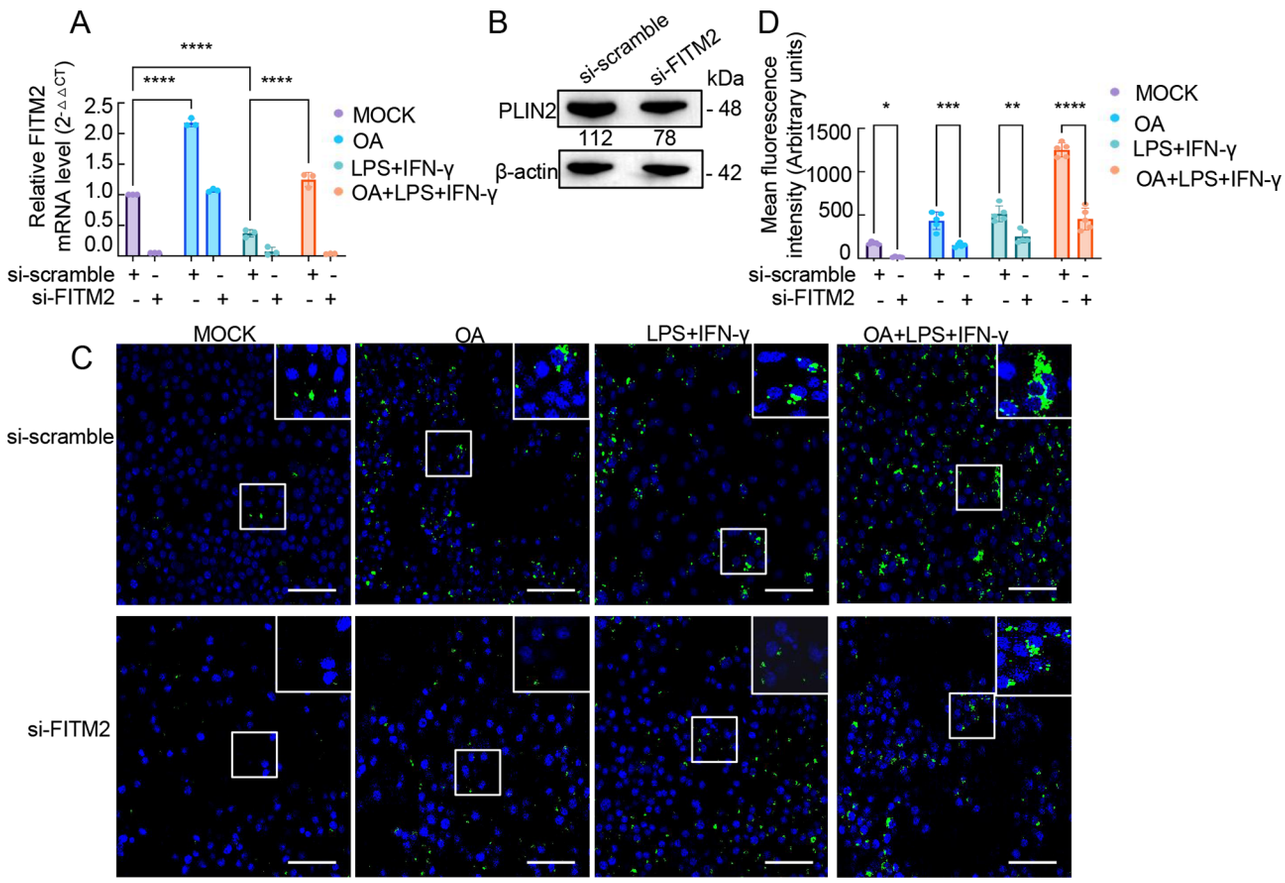

Figure 2 *FITM2*-mediated LD formation.

A: RT-qPCR analysis of FITM2 transcript levels in RAW264.7 cells transfected with si-*FITM2* or si-scramble and treated with LPS, IFN-γ, and OA. B: Western blot analysis of PLIN2, a marker of LDs, with β-actin as the internal control. C: Confocal microscopy images showing LD formation in *FITM2* knockdown and control cells. D: Quantification of BODIPY-stained LD fluorescence intensity using ImageJ. All images shown are representative of at least three independent experiments. Data are presented as mean±SD. (*n*=3). *: *P*<0.1; **: *P*<0.01; ***: *P*<0.001; ****: *P*<0.0001; ns: Not significant, two-way ANOVA.

and M2 markers were evaluated following stimulation with LPS and IFN-γ, with or without OA. *FITM2* knockdown markedly amplified M1 polarization, evidenced by a 10-fold increase in TNF-α, iNOS, and IL-6 transcription levels and a 1.5-fold decrease in CD206 and Arg-1 transcription levels in the LPS+IFN-γ and OA+LPS+IFN-γ groups compared with control cells (Figure 3A). Consistent with transcriptional changes, iNOS and TNF-α protein levels were elevated in *FITM2*-silenced cells, as confirmed by WB, while ELISA revealed significantly elevated secretion of TNF-α and IL-6 (Figure 3B–D). Furthermore, flow cytometry revealed elevated ROS levels and neutral red staining demonstrated increased lysosomal activity in *FITM2* knockdown cells compared to cells transfected with scrambled siRNA (Figure 3E, F). These findings demonstrate that *FITM2*-mediated LD biosynthesis inhibits M1 macrophage polarization.

RNA-seq reveals key LD-regulated genes involved in M1 macrophage polarization

To elucidate the transcriptional landscape underlying LD-regulated macrophage polarization, RNA-seq was performed on *FITM2*-silenced RAW264.7 cells co-stimulated with LPS and IFN-γ. Differentially expressed genes (DEGs) were defined by a fold change greater than 2 or less than 0.5 and a *P*-value less than 0.05. A total of 319 up-regulated and 202 down-regulated DEGs were identified in *FITM2* knockdown cells (Figure 4A; Supplementary Table S3). Kyoto Encyclopedia of Genes and Genomes (KEGG) pathway enrichment analysis revealed significant activation of immune-related signaling networks, including the PI3K-Akt and MAPK signaling pathways, along with enrichment in lipid metabolism and atherosclerosis-related pathways (Figure 4B). Gene Ontology (GO) analysis demonstrated enrichment in several immune-related pathways, including immune system processes and multiple responses to stress and stimuli (Figure 4C). Several LD-associated genes, including *FABP5*, *SCD2*, and *Hsd17b7*, were among the identified DEGs, alongside the targeted *FITM2* gene itself. RT-qPCR validation confirmed altered expression of these transcripts in *FITM2* knockdown cells (Figure 4D). Notably, OA treatment mitigated the down-regulation of *SCD2* and *Hsd17b7* in the *FITM2*-silenced context, suggesting lipid-driven compensatory effects. In contrast, *SCD1* expression was up-regulated in mock-transfected cells upon *FITM2* knockdown. Under combined stimulation with OA, LPS, and IFN-γ, only *FABP5* expression patterns consistently aligned with RNA-seq results, implicating *FABP5* as a core LD-responsive gene associated with M1 polarization.

FABP5 regulates LD abundance and M1 macrophage polarization

To elucidate the role of *FABP5* in M1 macrophage polarization, *FABP5* was knocked down in both wild-type and *FITM2*-deficient RAW264.7 cells. Confocal microscopy revealed that

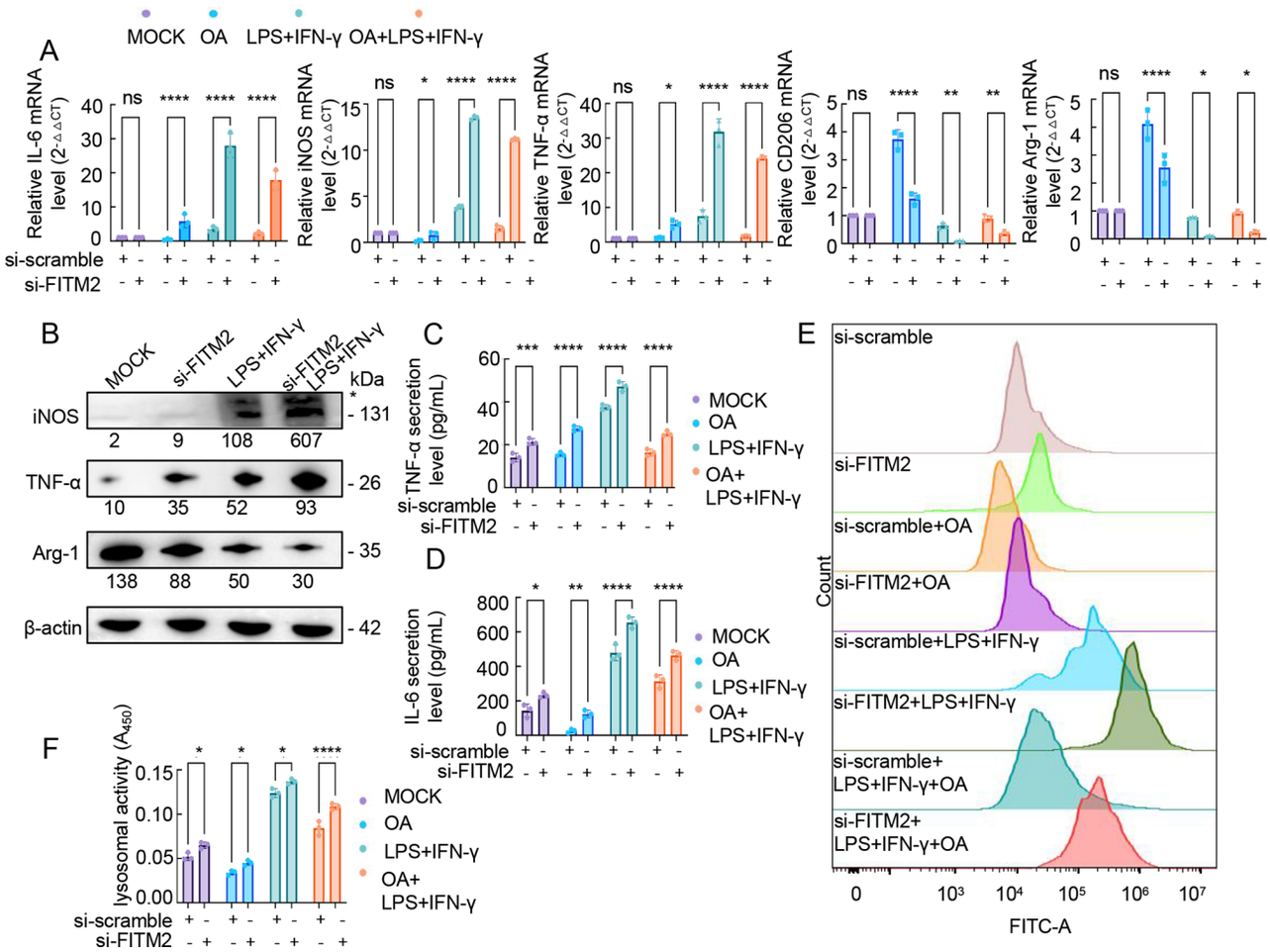

Figure 3 Inhibition of LD formation by si-*FITM2* enhances M1 macrophage polarization.

A: RT-qPCR analysis of M1 and M2 polarization marker transcripts in *FITM2* knockdown and control cells. B: Western blot analysis of polarization-related proteins, with β-actin as the internal control. C–D: ELISA quantification of TNF-α and IL-6 secretion. E: Flow cytometry analysis of intracellular ROS levels under indicated treatments. F: Lysosomal activity assessed by neutral red dye staining. Data are presented as mean±SD. (n=3). *: P<0.1; **: P<0.01; ***: P<0.001; ****: P<0.0001; ns: Not significant, two-way ANOVA.

FABP5 knockdown significantly reduced LD abundance, mirroring the effect of *FITM2* silencing. Simultaneous knockdown of *FITM2* and *FABP5* led to an even greater depletion of LDs (Figure 5A, B). Morphological examination further indicated an increase in M1-like cells in the dual knockdown group relative to single knockdown or control conditions (Figure 5C).

RT-qPCR was performed to quantify the transcripts of M1 markers (TNF-α, iNOS, and IL-6) and M2 markers (CD206 and Arg-1). Transcriptional profiling demonstrated that *FABP5* knockdown up-regulated TNF-α, iNOS, and IL-6 while down-regulating CD206 and Arg-1 (Figure 5D), consistent with enhanced M1 polarization. These transcriptomic changes were further amplified in cells transfected with both si-*FITM2* and si-*FABP5*. Both WB and ELISA confirmed the corresponding increases in TNF-α and iNOS protein levels, as well as elevated secretion of TNF-α and IL-6, with the highest levels observed in the dual knockdown group (Figure 5E–G).

To assess the functional consequences of FABP5 loss, intracellular ROS production and lysosomal activity were also measured. Flow cytometric analysis revealed that *FABP5* knockdown elevated ROS levels, and this effect was further amplified in cells lacking both *FITM2* and *FABP5* (Figure 5H). Similarly, neutral red staining revealed a parallel increase in lysosomal activity, with maximal enhancement in the co-knockdown condition (Figure 5I). Together, these findings indicate that FABP5 acts in concert with FIT2 and contributes to LD-mediated inhibition of M1 macrophage polarization.

FABP5- and FIT2-mediated LD abundance modulates macrophages antibacterial capacity

Given the established role of M1 polarization in host defense and the involvement of LDs in antimicrobial responses (Ivashkiv, 2013; Lumeng et al., 2007; Mina et al., 2024), the relationship between LD abundance, macrophage polarization, and bacterial phagocytosis was investigated. RAW264.7 cells were polarized toward an M1 phenotype using LPS and IFN-γ, followed by infection with *Edwardsiella piscicida* EIB202, *Salmonella enterica* subsp. *enterica* serovar Typhimurium SL1344, or *Escherichia coli* DH5α at an MOI of 10. Colony formation analysis demonstrated that M1-polarized macrophages exhibited a 3–4-fold increase in intracellular killing of *E. piscicida* and *S.* Typhimurium compared to non-polarized controls (Figure 6A). In time-course assays, *E. piscicida* replication steadily increased in unpolarized macrophages, whereas bacterial loads remained consistently low in M1-polarized cells (Figure 6B), indicating that M1 activation enhances macrophage-mediated restriction of intracellular

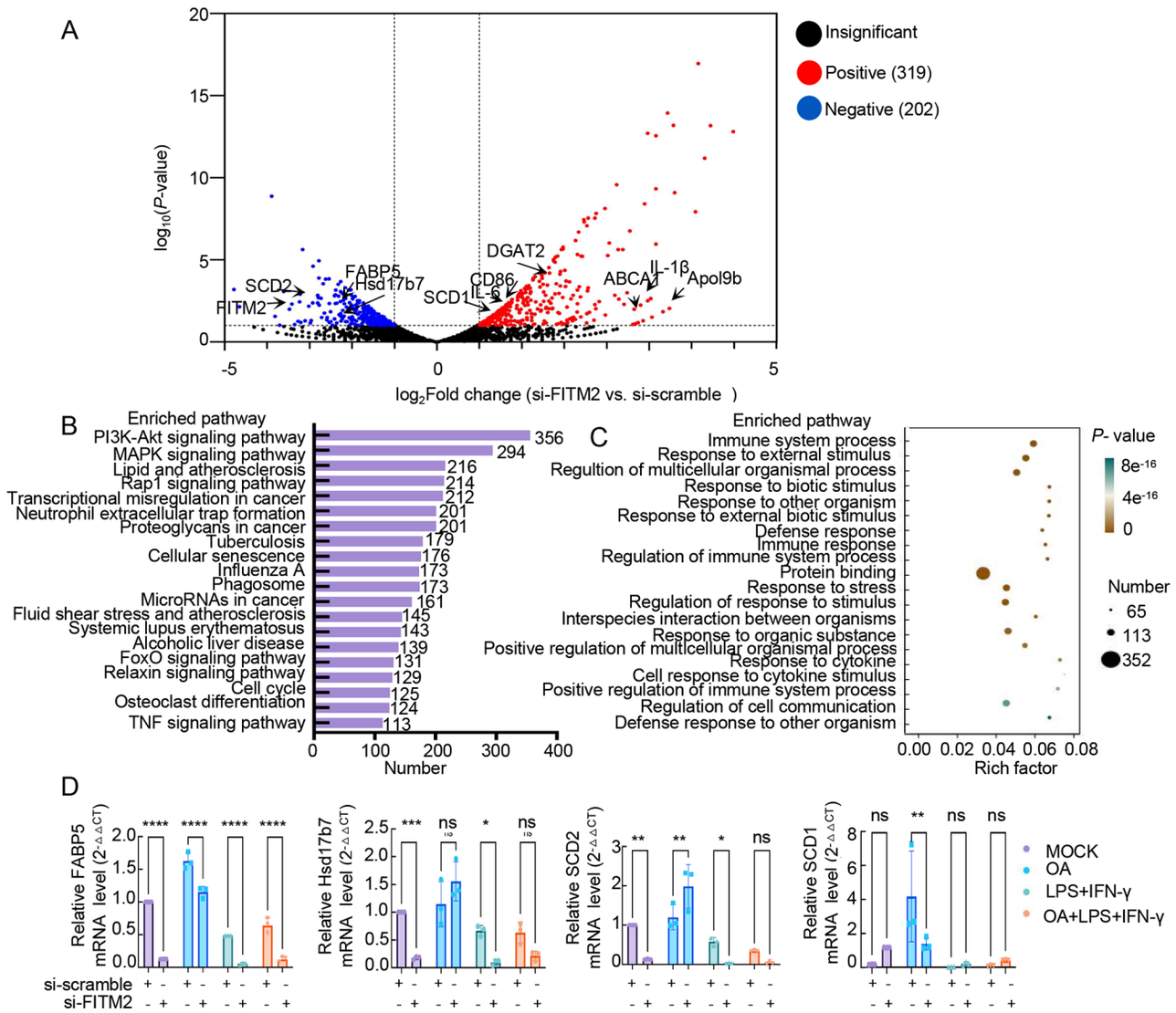

Figure 4 RNA-seq analysis identifies LD-regulated genes involved in M1 macrophage polarization.

A: RNA-seq was performed on *FITM2* knockdown and mock-transfected RAW264.7 cells after 12 h of treatment with LPS and IFN-γ. Differentially expressed genes (DEGs) were determined based on fold change >2 or <0.5 and P<0.05. B: KEGG pathway analysis of DEGs. C: Gene Ontology (GO) enrichment analysis of DEGs. D: RT-qPCR validation of *FABP5*, *Hsd17b7*, *SCD1*, and *SCD2* transcript levels in *FITM2* knockdown and mock cells treated with LPS, IFN-γ, and OA. Data are presented as mean±SD. (n=3). *: P<0.1; **: P<0.01; ***: P<0.001; ****: P<0.0001; ns: Not significant, two-way ANOVA.

pathogens. To assess LD dynamics during infection and polarization, LD abundance was quantified in macrophages stimulated with LPS and IFN-γ, and in wild-type cells infected with *S*. Typhimurium, *E. coli*, and *E. piscicida* (Figure 6C, D). Confocal microscopy revealed that LD levels increased following infection with *S.* Typhimurium and *E. piscicida*, whereas *E. coli* infection resulted in reduced LD content, suggesting pathogen-specific modulation of host lipid storage pathways.

To assess how LD accumulation affects macrophage bactericidal function, cells were treated with OA in combination with LPS and IFN-γ, followed by *E. piscicida* infection. Compared to LPS and IFN-γ treatment alone, OA co-treatment led to increased intracellular bacterial survival, suggesting that elevated LD levels may impair the phagocytic capacity of M1 macrophages (Figure 6E). To determine whether LD-associated proteins contribute to this effect, *FITM2* and *FABP5* were knocked down individually and in combination. Co-knockdown of *FITM2* and *FABP5* resulted in the greatest suppression of *E. piscicida* colonization (Figure 6F).

To further validate these findings, RAW264.7 macrophages were infected with mCherry-expressing *E. piscicida*, and bacterial colonization was assessed by fluorescence microscopy. Fluorescence intensity, serving as a proxy for viable intracellular bacteria, was inversely correlated with the degree of M1 polarization. In wild-type cells, LPS+IFN-γ treatment significantly reduced bacterial burden, whereas co-treatment with OA partially abolished this effect (Figure 6G). Moreover, in contrast to scrambled siRNA controls, co-knockdown of *FITM2* and *FABP5* led to near-complete clearance of *E. piscicida* (Figure 6H). Morphological analysis further showed that round-shaped macrophages, indicative of non-polarized or weakly polarized macrophages, exhibited stronger fluorescence signals than spindle-shaped M1-polarized cells. These findings indicate that M1 polarization enhances intracellular bacterial clearance, while LD

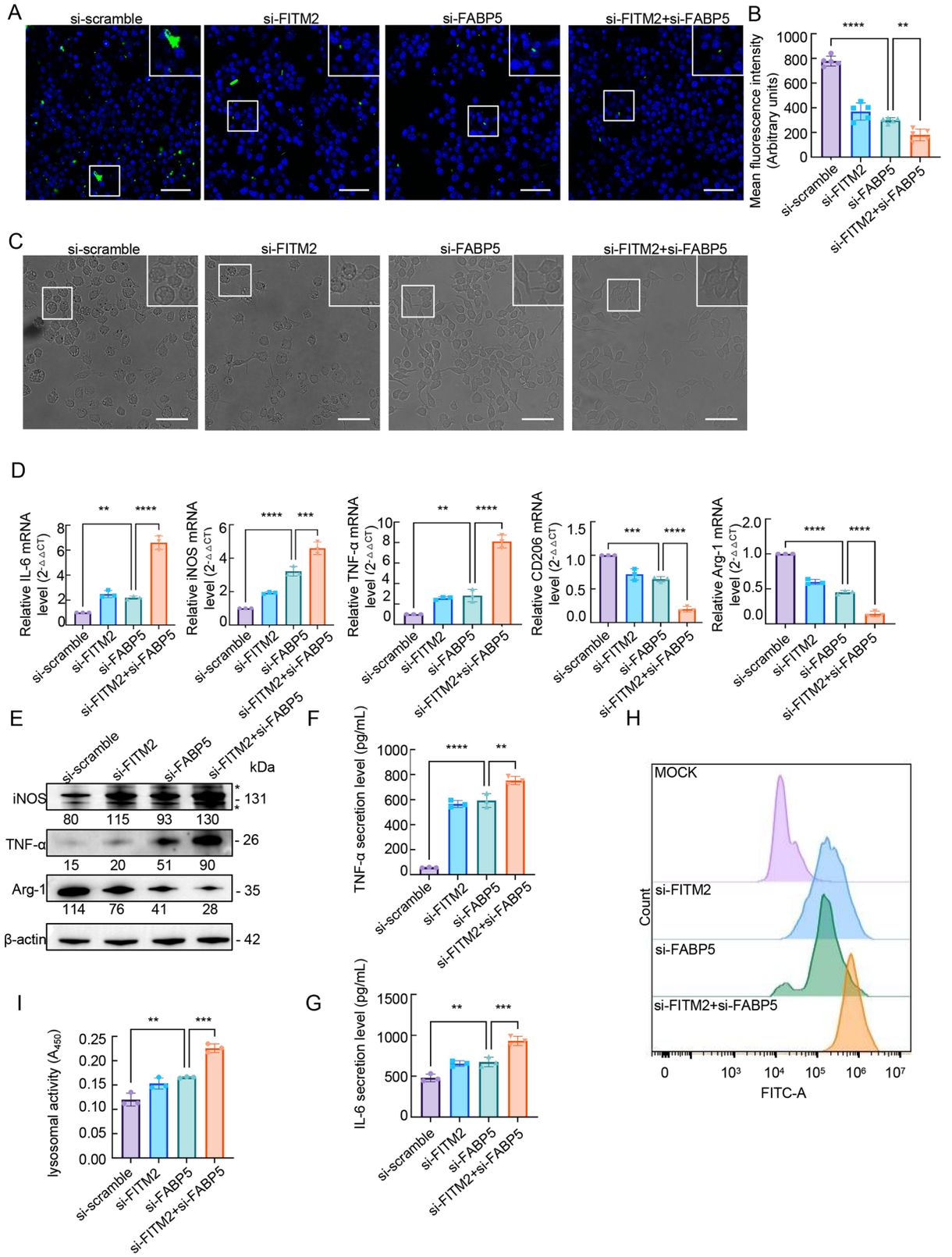

Figure 5 FABP5 modulates LD abundance and M1 macrophage polarization.

A: Confocal microscopy images of RAW264.7 cells showing LD abundance following knockdown of *FABP5* and *FITM2*. B: Quantification of BODIPY (green)-stained LD fluorescence intensity using ImageJ. C: Morphological analysis of cells transfected with si-*FABP5* and si-*FITM2*. Spindle-shaped morphology indicates M1 polarization. D: RT-qPCR analysis of M1 (TNF-α, iNOS, IL-6) and M2 (CD206, Arg-1) marker transcripts following *FABP5* knockdown. E: Western blot analysis of macrophage polarization markers; β-actin was used as internal control. F–G: ELISA quantification of secreted TNF-α and IL-6. H: Intracellular ROS levels assessed by flow cytometry. I: Lysosomal activity evaluated by neutral red dye staining. All images shown are representative of at least five independent experiments. Data are presented as mean±SD. (*n*=3). *: *P*<0.1; **: *P*<0.01; ***: *P*<0.001; ****: *P*<0.0001; ns: Not significant, two-way ANOVA.

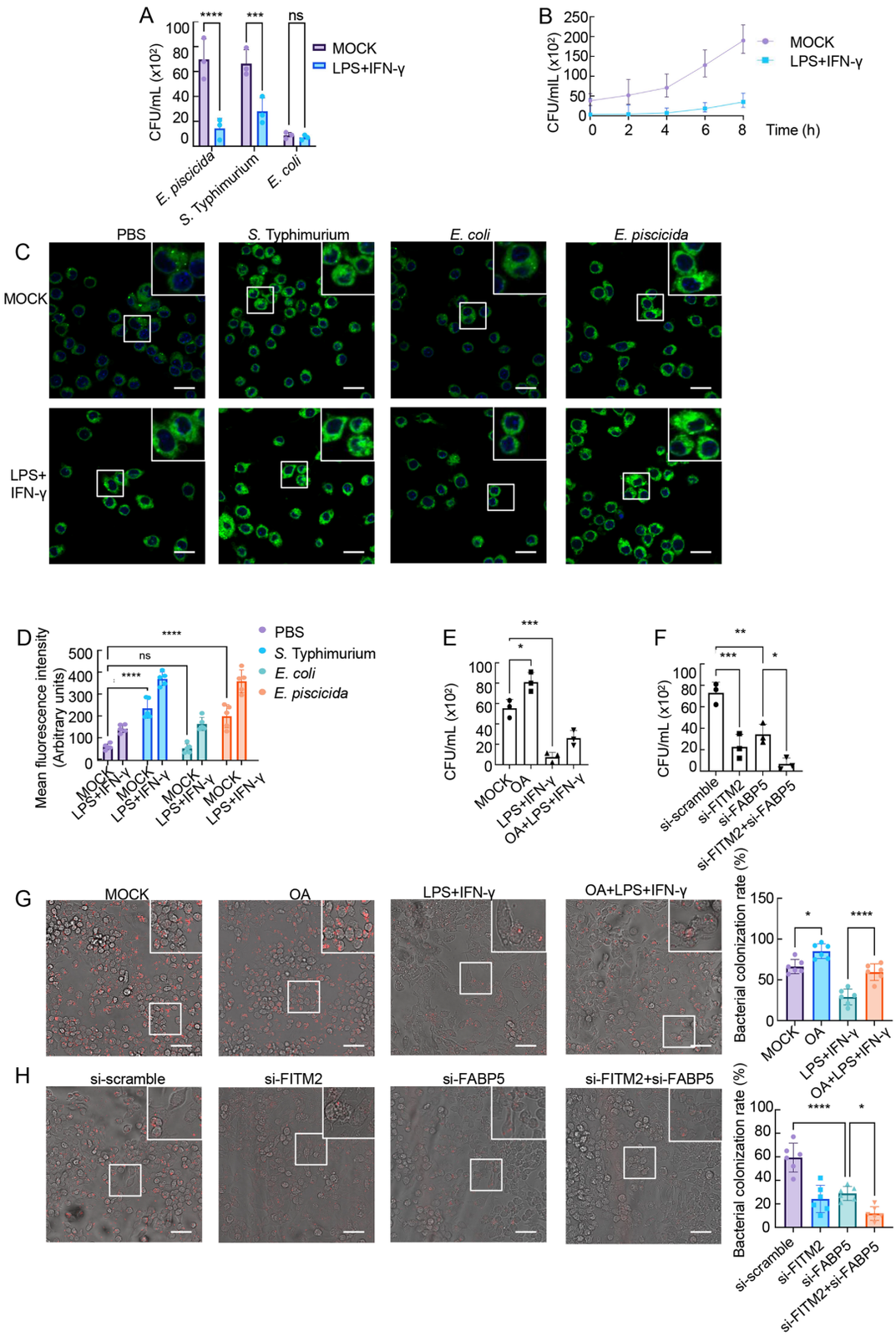

Figure 6 FABP5- and FIT2-mediated LD accumulation impairs macrophage capacity to eliminate intracellular pathogens.

A: RAW264.7 cells were infected with *E. piscicida* EIB202, *S.* Typhimurium SL1344, or *E. coli* DH5α at an MOI of 10. Intracellular bacterial loads at 4 h post-infection were normalized to cell numbers. B: LPS and IFN-γ treatment enhanced clearance of *E. piscicida* by macrophages. Intracellular bacterial load was normalized to cell number. C: Confocal microscopy images of LD abundance in *E. piscicida*-infected RAW264.7 cells. D: Quantification of BODIPY (green)-stained LD fluorescence using ImageJ. E–F: Intracellular survival of *E. piscicida* in RAW264.7 cells treated with LPS, IFN-γ, and OA (E) or in FITM2 and FABP5 knockdown cells (F). G–H: Mean fluorescence intensity (MFI) of *E. piscicida* expressing constitutive chromosomal mCherry in spindle-shaped (M1-like) versus round (less polarized) RAW264.7 cells treated with LPS, IFN-γ, and OA (G) or transfected with si-FITM2 and si-FABP5 (H). All images shown are representative of at least three independent experiments. Data are presented as mean±SD. *: P<0.1; **: P<0.01; ***: P<0.001; ****: P<0.0001; ns: Not significant, one-way ANOVA.

accumulation mediated by FIT2 and FABP5 inhibits this process by suppressing M1 polarization.

DISCUSSION

Macrophage function is largely dependent on its own cellular metabolism (O'Neill et al., 2016). Macrophages, as innate immune cells, undergo phenotypic polarization in response to microenvironmental stimuli and thus fulfill specific functions. In the present study, OA treatment markedly increased LD abundance while suppressing M1 polarization in RAW264.7 cells. Transcriptomic profiling of *FITM2* knockdown cells identified FABP5 as a downstream effector of LD biosynthesis-mediated immunomodulation. Impaired M1 polarization, driven by FIT2- and FABP5-dependent LD accumulation, corresponded with reduced intracellular killing of *E. piscicida* and *S.* Typhimurium, highlighting a metabolic mechanism that compromises macrophage resistance to pathogens.

Proinflammatory M1 polarization has been shown to induce lipid synthesis and LD accumulation in macrophages to facilitate defense against bacterial infection. Enhanced lipid synthesis supports the connection between the actin cytoskeletal network and plasma membrane, thereby enhancing phagocytosis (Lee et al., 2018b). Lipid remodeling also amplifies cytokine production and secretion, contributing to a robust inflammatory response (Yan & Horng, 2020). In addition, macrophages increase phosphatidylcholine synthesis during infection, activating the NLRP3 inflammasome pathway and inducing IL-1β and IL-18 production to promote host defense (Sanchez-Lopez et al., 2019).

However, LDs also serve as intracellular nutrient stores that can be exploited by pathogens to enhance their resilience against stressful environments (Hüsler et al., 2023). As immunometabolic hubs, LDs defend against pathogenic bacteria, responding to signals by reprogramming cell metabolism and eliciting protein-mediated antimicrobial mechanisms (Bosch et al., 2020). Given the role of FABP5 in LD metabolism, its contribution to pathogen resistance was further investigated. FABP5 deficiency in macrophages has been shown to increase IL-4-driven M2 polarization, accompanied by elevated intracellular levels of unsaturated long-chain fatty acids and enhanced fatty acid β-oxidation, tricarboxylic acid (TCA) cycle flux, and oxidative phosphorylation (Hou et al., 2022b). This metabolic shift supports an M2-like phenotype, in contrast to the glycolytic metabolism characteristic of M1 macrophages, which rely on aerobic glycolysis, increased glucose and glutamine uptake, and accumulation of citrate and succinate due to a disrupted TCA cycle (Viola et al., 2019; Yan and Horng, 2020). These findings underscore a functional interplay between FABP5 and LD dynamics in regulating macrophage polarization.

In the context of LPS and IFN-γ stimulation, *FITM2* knockdown altered the expression of numerous immune-associated pathways, including those involved in the MAPK, TGF-β, and TNF signaling pathways, all of which are implicated in M1 polarization dynamics (Jung et al., 2019). MAPK pathway components such as ERK, p38, and JNK modulate transcriptional activity of inflammatory regulators including NF-κB (Huang et al., 2019), while TNF-α and TGF-β serve as canonical indicators of M1 and M2 states, respectively. The findings presented here support a model in which LPS stimulation promotes fatty acid synthesis and FIT2-dependent LD formation. This LD expansion promotes *FABP5* transcription, which, in turn, reinforces LD biogenesis, constituting a positive feedback loop. The resulting LD accumulation attenuates M1 polarization and reduces macrophage antibacterial activity (Figure 7). Collectively, the

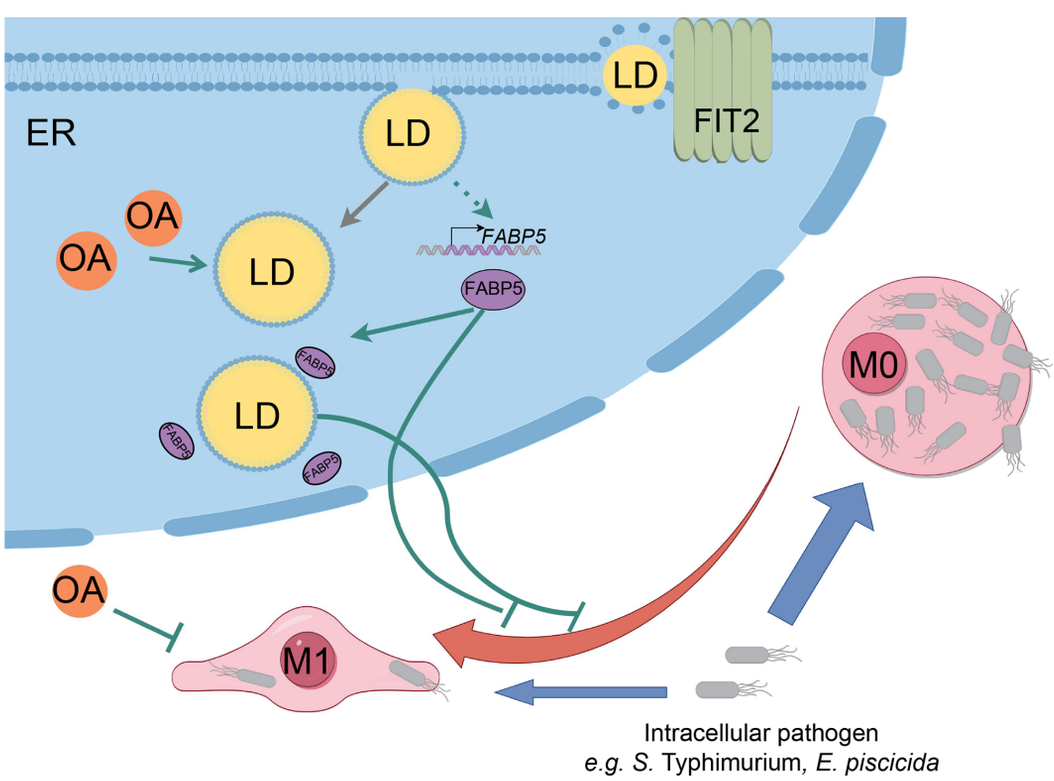

Figure 7 Schematic representation of LD-mediated suppression of M1 macrophage polarization and reduced resistance to bacterial invasion.

extent of M1 macrophage polarization plays a pivotal role in determining host resistance to intracellular pathogen invasion, offering potential avenues for therapeutic intervention and infectious disease control. Future investigations into M1 polarization across diverse animal models should account for context-dependent variation among tissues, organs, and species to better understand its contribution to antimicrobial defense.

DATA AVAILABILITY

The raw sequencing data are available from the NCBI database under BioProjectID PRJNA1184227, as well as the Genome Sequence Archive (https://ngdc.cncb.ac.cn/gsa) under accession number PRJCA039845 and Science Data Bank (https://www.scidb.cn/en; doi: 10.57760/sciencedb.j00139.00212).

SUPPLEMENTARY DATA

Supplementary data to this article can be found online.

COMPETING INTERESTS

The authors declare that they have no competing interests.

AUTHORS' CONTRIBUTIONS

Conceptualization: Q.Y.W; Data curation: Y.H.L S.S; Funding acquisition: Q.Y.W; Investigation: Y.H.L B.L; Project administration: Y.X.Z S.H.C; Supervision: Q.Y.W S.S; Validation: S.S; Visualization: Y.H.L B.L S.S; Writing – original draft: Y.H.L S.S; Writing – review and editing: S.S Q.Y.W. All authors read and approved the final version of the manuscript.

REFERENCES

Bosch M, Sánchez-Álvarez M, Fajardo A, et al. 2020. Mammalian lipid droplets are innate immune hubs integrating cell metabolism and host defense. *Science*, **370**(6514): eaay8085.

Boutilier AJ, Elsawa SF. 2021. Macrophage polarization states in the tumor microenvironment. *International Journal of Molecular Sciences*, **22**(13): 6995.

Chen F, Yan B, Ren J, et al. 2021. FIT2 organizes lipid droplet biogenesis with ER tubule-forming proteins and septins. *The Journal of Cell Biology*, **220**(5): e201907183.

Chen YN, Hu MR, Wang L, et al. 2020. Macrophage M1/M2 polarization. *European Journal of Pharmacology*, **877**: 173090.

Furuhashi M, Hotamisligil GS. 2008. Fatty acid-binding proteins: role in metabolic diseases and potential as drug targets. *Nature Reviews Drug Discovery*, **7**(6): 489–503.

Goeritzer M, Schlager S, Radovic B, et al. 2014. Deletion of CGI-58 or adipose triglyceride lipase differently affects macrophage function and atherosclerosis. *Journal of Lipid Research*, **55**(12): 2562–2575.

Griseti E, Bello AA, Bieth E, et al. 2024. Molecular mechanisms of perilipin protein function in lipid droplet metabolism. *Federation of European Biochemical Societies Letters*, **598**(10): 1170–1198.

Hou YX, Wei D, Bossila EA, et al. 2022a. FABP5 deficiency impaired macrophage inflammation by regulating AMPK/NF-κB signaling pathway. *The Journal of Immunology*, **209**(11): 2181–2191.

Hou YX, Wei D, Zhang ZQ, et al. 2022b. FABP5 controls macrophage alternative activation and allergic asthma by selectively programming long-chain unsaturated fatty acid metabolism. *Cell Reports*, **41**(7): 111668.

Huang SP, Guan X, Kai GY, et al. 2019. Broussonin E suppresses LPS-induced inflammatory response in macrophages via inhibiting MAPK pathway and enhancing JAK2-STAT3 pathway. *Chinese Journal of Natural Medicines*, **17**(5): 372–380.

Hüsler D, Stauffer P, Hilbi H. 2023. Tapping lipid droplets: a rich fat diet of intracellular bacterial pathogens. *Molecular Microbiology*, **120**(2): 194–209.

Ivashkiv LB. 2013. Epigenetic regulation of macrophage polarization and function. *Trends in Immunology*, **34**(5): 216–223.

Jung J, Zeng H, Horng T. 2019. Metabolism as a guiding force for immunity. *Nature Cell Biology*, **21**(1): 85–93.

Kadereit B, Kumar P, Wang WJ, et al. 2008. Evolutionarily conserved gene family important for fat storage. *Proceedings of the National Academy of Sciences of the United States of America*, **105**(1): 94–99.

Karanth S, Denovan-Wright EM, Thisse C, et al. 2008. The evolutionary relationship between the duplicated copies of the zebrafish *fabp11* gene and the tetrapod *FABP4, FABP5, FABP8* and *FABP9* genes. *The FEBS Journal*, **275**(12): 3031–3040.

Lee GS, Pan YJ, Scanlon MJ, et al. 2018a. Fatty acid-binding protein 5 mediates the uptake of fatty acids, but not drugs, into human brain endothelial cells. *Journal of Pharmaceutical Sciences*, **107**(4): 1185–1193.

Lee JH, Phelan P, Shin M, et al. 2018b. SREBP-1a-stimulated lipid synthesis is required for macrophage phagocytosis downstream of TLR4-directed mTORC1. *Proceedings of the National Academy of Sciences of the United States of America*, **115**(52): E12228–E12234.

Liang XM, Fu WL, Peng YH, et al. 2023. Lycorine induces apoptosis of acute myeloid leukemia cells and inhibits triglyceride production via binding and targeting FABP5. *Annals of Hematology*, **102**(5): 1073–1086.

Lumeng CN, Bodzin JL, Saltiel AR. 2007. Obesity induces a phenotypic switch in adipose tissue macrophage polarization. *The Journal of Clinical Investigation*, **117**(1): 175–184.

Manoharan RR, Prasad A, Pospíšil P, et al. 2024. ROS signaling in innate immunity via oxidative protein modifications. *Frontiers in Immunology*, **15**: 1359600.

Mina SA, Zhu GC, Fanian M, et al. 2024. Exploring reduced macrophage cell toxicity of hypervirulent *Klebsiella pneumoniae* compared to classical *Klebsiella pneumoniae*. *Microbiological Research*, **278**: 127515.

Noy R, Pollard JW. 2014. Tumor-associated macrophages: from mechanisms to therapy. *Immunity*, **41**(1): 49–61.

Olzmann JA, Carvalho P. 2019. Dynamics and functions of lipid droplets. *Nature Reviews Molecular Cell Biology*, **20**(3): 137–155.

O'Neill LAJ, Kishton RJ, Rathmell J. 2016. A guide to immunometabolism for immunologists. *Nature Reviews Immunology*, **16**(9): 553–565.

O'sullivan SE, Kaczocha M. 2020. FABP5 as a novel molecular target in prostate cancer. *Drug Discovery Today*, **25**(11): 2056–2061.

Russell DG, Huang L, VanderVen BC. 2019. Immunometabolism at the interface between macrophages and pathogens. *Nature Reviews Immunology*, **19**(5): 291–304.

Sanchez-Lopez E, Zhong ZY, Stubelius A, et al. 2019. Choline uptake and metabolism modulate macrophage IL-1β and IL-18 production. *Cell Metabolism*, **29**(6): 1350–1362. e7.

Sergin I, Evans TD, Razani B. 2015. Degradation and beyond: the macrophage lysosome as a nexus for nutrient sensing and processing in atherosclerosis. *Current Opinion in Lipidology*, **26**(5): 394–404.

Sica A, Mantovani A. 2012. Macrophage plasticity and polarization: in vivo veritas. *The Journal of Clinical Investigation*, **122**(3): 787–795.

Song JR, Zhang YL, Frieler RA, et al. 2023. Itaconate suppresses atherosclerosis by activating a Nrf2-dependent antiinflammatory response in macrophages in mice. *The Journal of Clinical Investigation*, **134**(3): e173034.

Viola A, Munari F, Sánchez-Rodríguez R, et al. 2019. The metabolic

signature of macrophage responses. *Frontiers in Immunology*, **10**: 1462.

Walther TC, Chung J, Farese RV Jr. 2017. Lipid droplet biogenesis. *Annual Review of Cell and Developmental Biology*, **33**: 491–510.

Yan JW, Horng T. 2020. Lipid metabolism in regulation of macrophage functions. *Trends in Cell Biology*, **30**(12): 979–989.

Zechner R, Zimmermann R, Eichmann TO, et al. 2012. FAT SIGNALS-lipases and lipolysis in lipid metabolism and signaling. *Cell Metabolism*, **15**(3): 279–291.

Zhang CY, Yang L, Ding YF, et al. 2017. Bacterial lipid droplets bind to DNA via an intermediary protein that enhances survival under stress. *Nature Communications*, **8**: 15979.

Zhou LK, Lu Y, Qiu XX, et al. 2025. Lipid droplet efferocytosis attenuates proinflammatory signaling in macrophages via TREM2- and MS4A7-dependent mechanisms. *Cell Reports*, **44**(2): 115310.